Near Surface Properties of Mixtures of Propylammonium Nitrate with n-Alkanols 1. Nanostructure

Aaron Elbourne,[1] Samuel Cronshaw,[1] Kislon Voïtchovsky,[2] Gregory G. Warr,[3] and Rob Atkin[1,*]

[1] Discipline of Chemistry, The University of Newcastle, NSW 2308, Callaghan, Australia.

[2] Department of Physics, Durham University, Durham, England, United Kingdom.

[3] School of Chemistry, The University of Sydney, NSW 2006, Australia.

* Corresponding author

Abstract

In situ amplitude modulated - atomic force microscopy (AM-AFM) has been used to probe the nanostructure of mixtures of propylammonium nitrate (PAN) with n-alkanols near a mica surface. PAN is a protic ionic liquid (IL) which has a bicontinuous sponge-like nanostructure of polar and apolar domains in the bulk, which becomes flatter near a solid surface. Mixtures of PAN with 1-butanol, 1-octanol, and 1-dodecanol at 10 - 70 vol% n-alkanol have been examined, along with each pure n-alkanol, to reveal the effect of composition and n-alkanol chain length. At low concentrations the butanol simply swells the PAN near-surface nanostructure, but at higher concentrations the nanostructure fragments. Octanol and dodecanol first lower the preferred curvature of the PAN near-surface nanostructure because, unlike n-butanol, their alkyl chains are too long to be accommodated alongside the PAN cations. At higher concentrations, octanol and dodecanol self-assemble into n-alkanol rich aggregates in a PAN rich matrix. The concentration at which aggregation first becomes apparent decreases with n-alkanol chain length.

Introduction

Ionic liquids (ILs) are pure salts with melting points below 100 °C.[1-4] Unlike conventional molten solvents, many aprotic and protic ILs (PILs) have well-defined bulk-liquid nanostructures.[2] IL nanostructure was initially predicted from molecular dynamic simulations[5] and then later confirmed by radiation scattering.[6-9] Bulk IL nanostructure is a consequence of strong electrostatic attractions between the cations and anions, which form polar domains. Cation alkyl chains are solvophobically[6] excluded from the polar regions and cluster together to produce apolar regions.[2] The polar and apolar regions percolate through the bulk liquid in a bicontinous bulk structure reminiscent of an L_3 sponge. Similarly, radiation scattering studies have shown that pure primary n-alkanols (n = C_1 to C_{10}) have locally bilayered nanostructures, also due to amphiphilic effects.[10, 11] We have recently shown by small-angle X-ray scattering[12] that medium chain length n-alkanols form micelle-like and microemulsion-like nanostructures when mixed with PAN. The structure present depends on the n-alkanol chain length and concentration. This result is striking as n-alkanols do not aggregate in water.

When a pure IL contacts a solid surface the bulk nanostructure rearranges to form a new, but related, interfacial structure that is a compromise between the organisation imposed by both the specific chemistry and the planar geometry of flat, solid surface and the bulk liquid nanostructure.[13] Rearrangements are most severe for the ions in direct contact with the surface (the adsorbed or Stern layer). This decays over several nanometres (near surface region) into the bulk structure; the near surface nanostructure is templated by the surface bound ions but the templating effect decays rapidly with distance.

While the near-surface structure of ILs normal to solid interfaces is reasonably well understood,[13] this is not true of the lateral nanostructure, largely because it is more difficult to probe *in situ*. Lateral IL nanostructure at solid surfaces has been predicted from a variety of simulations[14-27] but there are few experimental reports. Scanning tunneling microscopy (STM)[28-30] has been employed to image IL interfacial structures, however, only the ion layer in direct contact with the surface has been imaged, and generally under very specific, somewhat artificial conditions (e.g. low temperature, ultra high vacuum, monolayer deposition or adsorption). These conditions are required to overcome interference from the near-surface IL-solid

interfacial structure which convolutes the tunneling current.[31, 32] Recently, we have used amplitude modulated atomic force microscopy (AM-AFM) imaging to examine the lateral IL-solid interface in contact with a bulk IL. A rich library of nanostructures were observed both adsorbed onto[33-37] and near[33, 36] solid interfaces, which revealed that previous descriptions based on data *normal* to the IL-solid interface were far too simplistic.[38-41] The nanostructure of the ion layer in contact with the substrate is strongly affected by the registry between the ions and surface adsorption sites,[13, 33-37] except when the cation is large and sterically hindered.[33] As in the bulk, near surface nanostructure is sensitive to both cation and anion type. For propylammonium nitrate (PAN), the bicontinuous, isotropic bulk sponge structure becomes flatter near a mica surface. Laterally extended polar surface domains are formed by propylammoniun ions electrostatically adsorbed to surface charge sites and additional cations solvophobically attracted to them. As the distance from the surface is increased, these large polar regions decay to the smaller, more highly-curved bulk structure.[33]

In this study the nanostructure of binary mixtures of PAN with butanol, octanol and dodecanol near a mica surface are investigated using AM-AFM as a function of composition. This reveals how the near surface nanostructure varies with liquid composition and n-alkanol alkyl chain length, with particular focus on the near surface region.

Methods

PAN was prepared via a 1:1 molar acid-base reaction. Slow addition of concentrated nitric acid (HNO_3) (AJAX Finechem Pty. Ltd, 70% w/w) to a chilled solution (<10°C) of hydrogenous propylamine (Aldrich 99% w/w%) and milli-Q water. During the acid addition, the mixture was stirred rapidly, in ice, to ensure dispersal of any heat generated. The resultant solution was first rotary evaporated for several hours and heated to 40°C. The sample was then thoroughly purged with nitrogen to prevent impurity formation (nitrous oxides or amides) and heated overnight in an oil bath at 105°C under a nitrogen atmosphere to remove remaining water. The water content of the IL was undetectable by Karl Fisher titration (<0.01 v/v%). Mica (muscovite) (Brown Co., Sydney) was prepared, just before experimentation, using adhesive tape to cleave along the silicates basal plane. The freshly cleaved mica was atomically smooth and clean.

1-butanol, 1-octanol, and 1-dodecanol were purchased from Sigma Aldrich (>97% purity). The PAN:alkanol mixtures were prepared at alkanol concentrations of 10, 30, 50 and 70% v/v by mass, assuming negligible volumes of mixing. The water content of each mixture was measured by Karl-Fisher titration to be <0.01 v/v % water.

The solutions were studied using an Asylum Research Cypher Atomic Force Microscope (Cypher AFM). All data was obtained at a constant temperature of 25°C via AM-AFM with the cantilevers oscillating at (or close to) resonant frequency. Soft cantilevers (BL-AC40TS, Olympus, Japan, nominal spring constant k_c = 0.25 N m^{-1}) were used to image the near surface nanostructure and surface-adsorbed ions are probed with stiff cantilevers (k = 6 N/m). Cantilever tips were irradiated with UV light for 15 minutes prior to each experiment to remove organic contaminants.[42] Each cantilever was calibrated using its thermal spectrum *in situ* prior to imaging and the lever sensitivity determined using force spectroscopy.[43] The experiments were completed in a droplet exposed to the atmosphere within the AFM (a sealed enclosure). As PAN and its mixtures with n-alkanols are hygroscopic, the water content of the liquid may increase during an experiment. The data presented here was obtained no more than 30 minutes after placing the IL droplet on the surface, and Karl Fischer titration verified that water contents were <1 wt% . The features of all images presented rotated as the scan angle was changed and scaled correctly with scan size, confirming they are not imaging artefacts.

AM – AFM topography images are obtained by applying a set working amplitude (A_0) (set-point) to the cantilever which is lower than the free oscillation amplitude (A). The sample is scanned line-by-line to produce a topographic image via the AFM feedback loop; the feedback loop maintains the set-point by continually adjusting the tip-sample distance in response to surface interactions. The near-surface or surface adsorbed layer is preferentially imaged via manipulating the cantilever imaging force, achieved by using cantilevers of differing spring constants and decreasing (near-surface regime) or increasing (adsorbed regime) the imaging set-point (A/A_0). Near-surface images were obtained with soft cantilevers (k = 0.25 N/m) using imaging conditions of A/A_0 = ~0.85, while surface-adsorbed ions are probed with stiff

cantilevers (k = 6 N/m, A/A_0 = ~0.7). In this way, the AFM tip is able to selectively probe the interfacial structure without contacting the mica substrate.

Average sizes for the features in the images were determined by measuring the length of the structures in 4 directions in three different images, obtained with different tips. The aggregate size was consistent between different tips, making a reverse imaging effect unlikely. The standard deviation of the feature dimensions given are ~ 10%.

Results and Discussion

The focus of this work is how the near surface nanostructure of PAN – n-alkanol mixtures depends on composition and n-alkanol chain length. However, because the near surface structure of pure ILs is templated by the morphology of the ion layer adsorbed to the surface, the structure of the ion layer adsorbed to the mica surface is first probed to determine any changes that occur upon n-alkanol addition.

Figure 1 compares topographic images of mica surfaces with pure PAN with those of PAN + 70 vol% n-alkanol. 70 vol% is the highest n-alkanol concentration investigated aside from the pure n-alkanols. Stiff cantilevers (k = 6 N/m) are used to minimise interference from the near surface structure. In an AM-AFM topographic image the dark areas indicate material between the cantilever tip and the surface which is relatively compliant (mobile), while lighter areas indicate noncompliant (more rigid) matter.[44]

Figure 1 A is consistent with images for the pure PAN – mica interface we have reported previously.[33] A well-defined lattice structure is clear, obscured in some areas by interference from near surface features. Although one row direction appears to dominate the image, the adsorbed layer in fact has hexagonal symmetry (indicated by the blue lines on the image) with a repeat spacing of ~0.5 nm, confirmed by fast Fourier transform (FFT),[45] shown as an inset. This repeat spacing is consistent with the lattice spacing of the underlying mica (0.52 nm)[46], within experimental error, and with previous studies of the protic IL-mica interface. It is produced by propylammonium cations electrostatically bound to the oxygen triads[47] associated with negatively charged mica surface sites.[33, 36, 37]

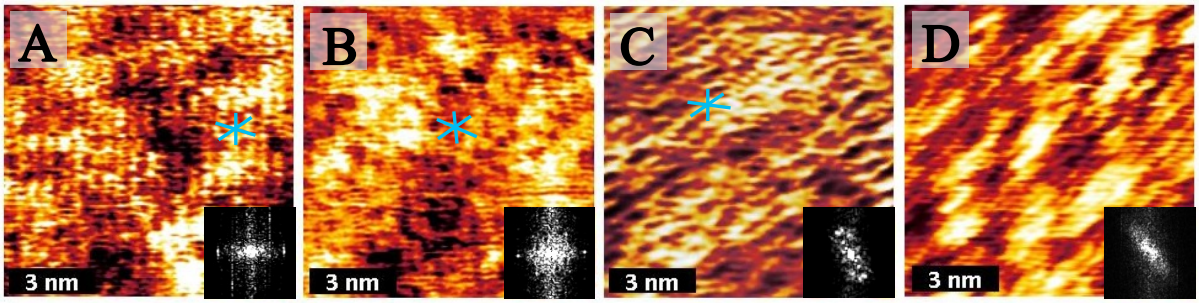

Figure 1. AM-AFM images of the ion layer adsorbed to the mica surface for pure PAN and the PAN / n-alkanol mixtures. (A) pure PAN, and 70 vol% (B) 1-butanol, (C) 1-octanol, and (D) 1-dodecanol in PAN. The slow scan direction in all cases is down the image.

Images of the adsorbed layer for mixtures of PAN + 70 vol% n-alkanol are presented in Figures 1 B (butanol), C (octanol) and D (dodecanol). Critically, even with 70 vol% n-alkanol, propylammonium rows are apparent for each system. This is because the propylammonium cation binds electrostatically to negatively charged adsorption sites on the mica, and the n-alkanols are unable to compete; n-alkanols can adsorb to oxygens on the mica surface via hydrogen bonds, but hydrogen bonds are typically an order of magnitude lower energy than electrostatic interactions.

The 70 vol% butanol image appears most similar to that of pure PAN, with clear hexagonal symmetry (blue lines) retained, but rows become less clear with longer n-alkanols. The rows are obscured for 70 vol% octanol system, but the three symmetry directions of the underlying mica lattice can still be discerned. Only one symmetry direction is apparent for PAN with 70 vol% dodecanol. This change might be attributed to the higher dodecanol viscosity hindering imaging, however, this is at odds with the clear images seen in pure PAN, which has a much higher viscosity[48] than either dodecanol[49] or PAN + dodecanol mixtures.[50] Dodecanol might also be solvophobically adsorbed to the solution-facing propyl chains of the adsorbed cations, which would hinder imaging; solvophobic attractions would be strongest for dodecanol due to its long alkyl chain, and decrease in strength as alkyl chain length is decreased. However, boundary layer shear force data shows no dependence on n-alkanol chain length, which makes this scenario unlikely.[50] The most probable cause of the decrease in image clarity with n-alkanol alkyl chain length is interference from near surface structure. The AM-AFM images for the near surface structures of PAN + 70 vol% n-alkanols show that near surface structure becomes larger and better defined as the n-alkanol chain length is increased. The physical size of these structures interferes with the AM-AFM tip during imaging of the adsorbed layer which

reduces clarity (*vide infra*). However, for all PAN + 70 vol% n-alkanol systems row features are clear and their spacing (0.5 nm) is commensurate with that for pure PAN and the mica lattice (within error). This confirms that that propylammonium adsorbs to surface charge sites from the PAN + vol% n-alkanol mixtures.

As cation rows, like those for pure PAN, are seen in all the n-alkanol mixtures at the highest mixture concentration studied, it is reasonable to assume that cations are also bound to the mica surface at all lower n-alkanol concentrations.

Figure 2 shows 40 nm × 40 nm AM-AFM topographic images in which the near surface structure has been selectively imaged using soft cantilevers (k = 0.25 N/m). Columns 1, 2 and 3 shows the PAN/butanol - mica, PAN/octanol - mica and PAN/dodecanol - mica systems, respectively, with the corresponding compositions of n-alkanol indicated. The features of these images are much larger than those for the corresponding adsorbed layer (c.f Figure 1), confirming that it is the near surface structure that is probed.

The near surface structures of the mixtures are markedly different to those of pure PAN indicating the presence of dissolved n-alkanol in the near-surface layers. Images for the pure PAN – mica interface have been reported previously,[33] and revealed areas of compliant and noncompliant domains in a sponge structure, reminiscent of the bulk morphology,[8] but more extended laterally than in the bulk. The noncompliant regions are ascribed to the polar domain, where electrostatic and hydrogen bonding interactions between charged groups lead to strong liquid cohesion. The compliant regions are therefore the aggregated cation alkyl chains.

As AM-AFM images of the near surface region discriminate between the polar and apolar domains, interpretation of the images in Figure 2 requires that the variation in apolar to polar volume fractions with as a function of liquid composition is known. Although we do not know how individual components are partitioned between these domains, the polar and apolar volume fractions of the components can be calculated according to:

$$[X_{PAN}\times(NO_3 + -NH_3) + X_{n-alkanol}\times(-OH)] : [X_{PAN}\times(-C_3H_7) + X_{n-alkanol}\times(-C_nH_{2n+1})] \quad \ldots (1)$$

where X_{PAN} is the mole fraction of PAN, $X_{n\text{-}alkanol}$ is the mole fraction of n-alkanol, (NO_3^- + $-NH_3^+$) is the volume of the PAN charged groups (68 Å^3)[51], ($-$OH) is the volume of the hydroxyl group (20 Å^3),[51] ($-C_3H_7$) is the volume of the PAN hydrocarbon chain (107 Å^3),[51] and ($-C_nH_{2n+1}$) is the volume of the n-alkanol group hydrocarbon chain as determined from the Tanford equation.[52]

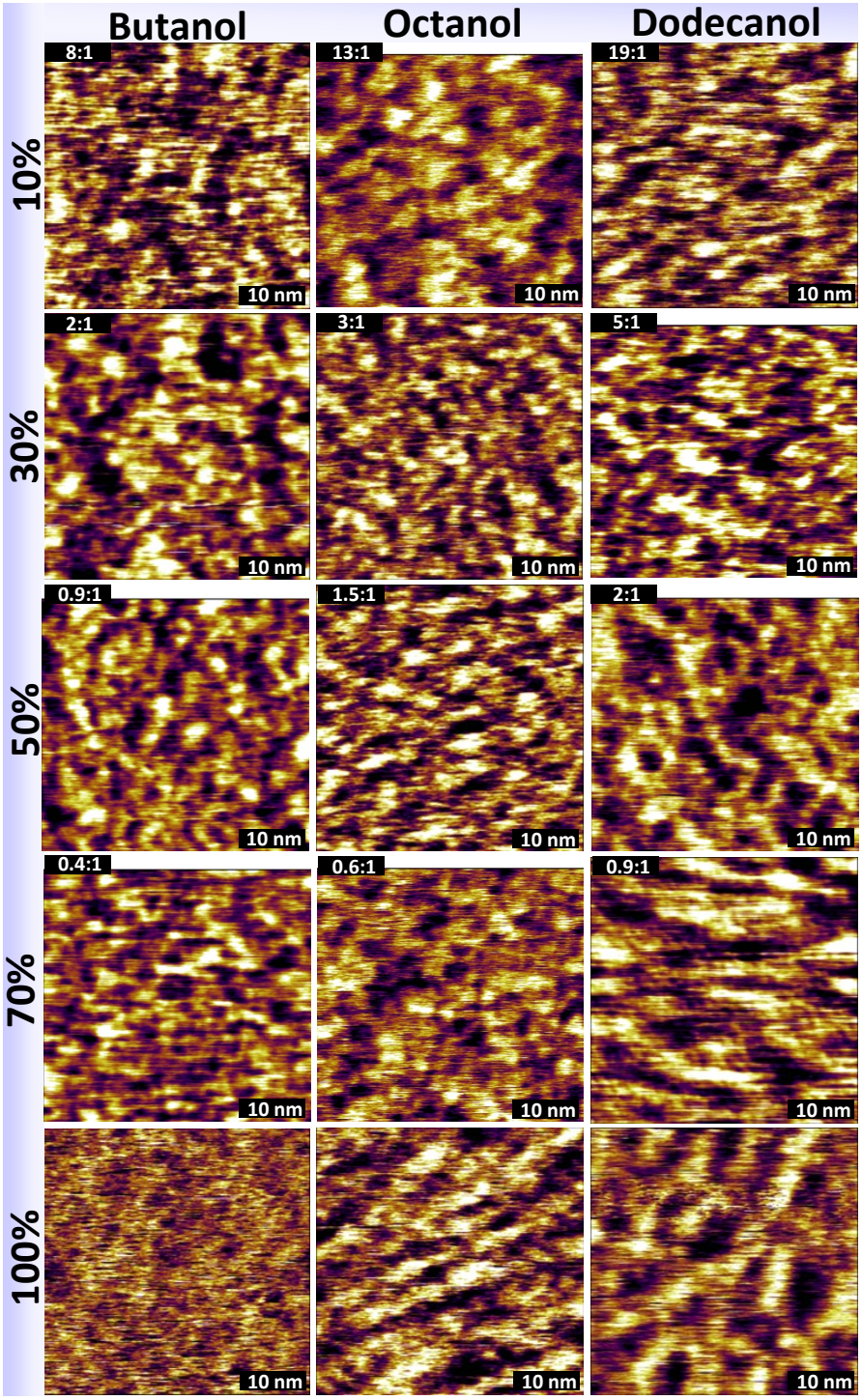

Figure 2. 40 nm x 40 nm topographical AM-AFM images of the near-surface layer of PAN:n-alkanol mixtures. Columns 1-3 show topographical images for 1-butanol, 1-octanol and 1-dodecanol, respectively. The alkanol content (vol%) increases down a column as indicated. The inset in the top left of each image shows the PAN: n-alkanol molecule ratio.

These values are listed in Table 1. As the polar group of the n-alkanols (the alcohol moeity) is smaller than the polar part of a PAN ion pair (ammonium group plus nitrate ion), and the hydrocarbon group of the n-alkanols are all larger than that of PAN, addition of butanol, octanol or dodecanol always increases the apolar vol : polar vol.

Table 1. n-Alkanol vol%, ratio of PAN ion pairs to n-alkanol molecules, volume fraction of polar groups (n-alkanol OH + PAN ammonium + nitrate) to apolar groups (n-alkanol hydrocarbon chain + PAN hydrocarbon chain), average near surface polar domain size and polar domain centre to centre distance for PAN / n-alkanol mixtures, pure PAN and pure n-alkanols.

	n-Alkanol vol%	PAN ion pairs: n-Alkanol molecules	Apolar vol : Polar vol.
Pure PAN	0	-	1.5:1
PAN / Butanol	10	8 : 1	1.7 : 1
	30	2 : 1	2.2 : 1
	50	0.9 : 1	2.8 : 1
	70	0.4 : 1	3.7 : 1
	100	-	7.1 : 1
PAN / Octanol	10	13 : 1	1.9 : 1
	30	3 : 1	2.8 : 1
	50	1.5 : 1	4.2 : 1
	70	0.6 : 1	6.5 : 1
	100	-	12.1 : 1
PAN / Dodecanol	10	19 : 1	2.1 : 1
	30	5 : 1	3.3 : 1
	50	2 : 1	5.0 : 1
	70	0.9 : 1	7.6 : 1
	100	-	15.4 : 1

The calculated apolar vol : polar vol ratio is a convenient measure of the relative amount of each material at each composition, and provides an upper bound on the ratio of light (polar) and dark (apolar) regions that could potentially be seen in the AM-AFM images in Figure 2 if the polar and apolar domains are completely segregated. In practice, we do not expect the polar and apolar moieties of the alcohols to be fully segregated.

The mean size of aggregates was calculated by measuring the lengths of all the structures in 4 directions in three different images and taking the average. A similar approach was used to determine the average center to center distance between astructures. These data are presented in Figure 3 as a function of the apolar vol: polar vol presented in Table 1. While trends are similar, the bulk liquid repeat spacing determined from the

peak position in SAXS data for the same system[12] is also presented in Figure 3. Notably, the centre to centre distances for near surface structures are significantly larger than the bulk liquid repeat spacing. This is consistent with the bulk liquid nanostructure becoming flatter near the mica.

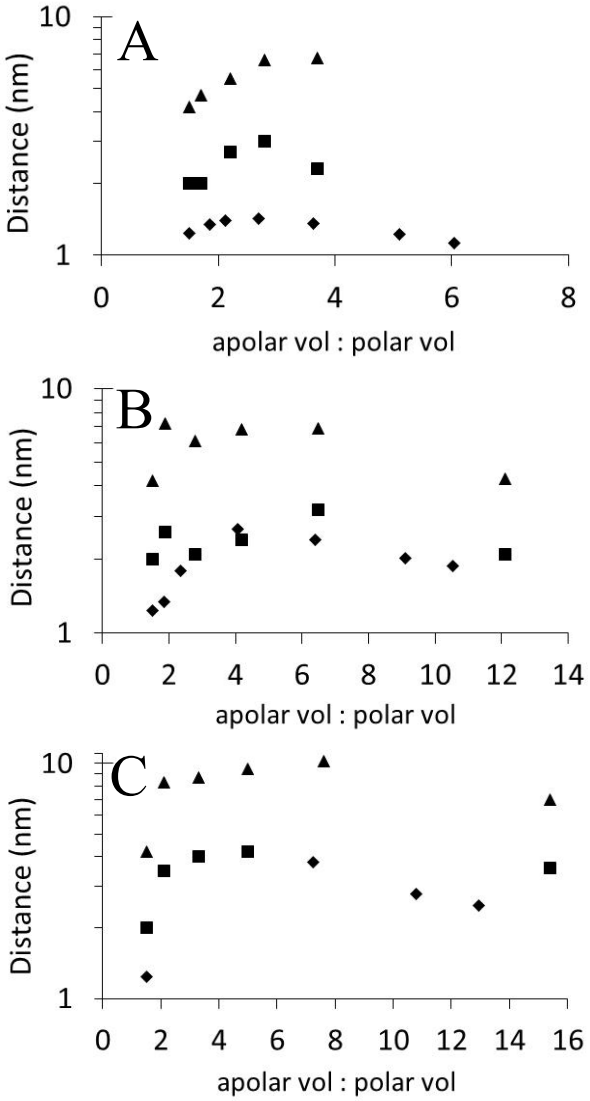

Figure 3. Near surface polar domain size (■) (nm), polar domain centre to centre distance (▲) (nm), and bulk liquid repeat spacing (♦) (nm) of A) butanol-, B) octanol- and C) dodecanol- PAN as a function of apolar vol : polar vol.

The appearance of the AM-AFM image for PAN + 10 vol% butanol is quite similar to that of pure PAN.[33] This is consistent with the bulk phase SAXS patterns which show that the addition of 10 vol% butanol to PAN hardly effects nanostructure, and with the modest change in the apolar vol : polar vol from 1.5:1 for pure PAN to 1.7:1 for PAN with 10 vol% butanol (Table 1). The average size of the (light) firm domains in the 10 vol% butanol image is ~2 nm, consistent with pure PAN, but the dark (compliant) regions appear

somewhat more interconnected, also consistent with the slightly increased apolar volume. This effect could also account for the weak low q scattering noted in the bulk SAXS data.[12]

Increasing butanol content to 30 vol% and beyond substantially alters the near-surface structure. The average diameter of the noncompliant polar regions has increased in size to 2.7 nm, the connectivity between these regions is lower, and the average centre to centre distance between polar domains has also increased by more than 1 nm compared to pure PAN. Corresponding effects are noted in the bulk phase X-ray scattering data in which the pre-peak, which is the signature of self-assembled IL nanostructure,[53] shifts to lower q, and the intensity of low q scattering increases.

When the butanol concentration is increased to 50 vol% the average size of the polar domains increases marginally to 3 nm but the centre to centre spacing increases strongly to 6.6 nm. The area of polar domains (bright) in the image is decreased compared to PAN + 30 vol% butanol, and the polar domains are even less interconnected; discrete polar domains completely surrounded by apolar (dark) regions are clear in parts of the image. These results are in keeping with the trend of apolar: polar volume ratio increasing with butanol content.

The appearance of the image changes markedly when the butanol concentration is increased to 70 vol%. Compared to the 50 vol% butanol image, the size of the polar (bright) domains is decreased to 2.3 nm while the spacing between polar domains remains essentially unchanged, *c.f.* Figure 3. The fact that the size of the polar domain decreases for 70 vol% butanol (as opposed to increasing with butanol vol% for all lower concentrations) shows that the native PAN nanostructure has been broken, and the solution consists of isolated PAN rich clusters dispersed in a butanol rich continuous phase. The increased area of compliant domains is in accordance with the higher apolar vol : polar vol of 3.7:1 (Table 1), and all of these results are consistent with the bulk X-ray scattering spectra where the pre-peak shifts back to higher Q (indicating smaller correlation lengths, c.f. Figure 3) and the intensity of low Q scattering decreases.

Subtle hints of structure are noted in the pure butanol images. This structure is due to undulations in the native butanol layers confined between the surface and the tip; this interpretation is made primarily on the

bases of the images for pure octanol and dodecanol, where the undulations are much clearer. The n-alkanols all form locally bilayered sheets in the bulk[10, 54, 55] which are aligned by the solid interface into smectic type layers.[56, 57] The strength of attractive interactions between n-alkanol hydrocarbon chains increases with chain length meaning that nanostructure becomes better defined, as seen in Figure 2, where the undulations are clearest for dodecanol, then octanol, and quite unclear for butanol. The undulation period increases with n-alkanol hydrocarbon chain length from 4.3 nm for butanol to 7 nm for dodecanol, consistent with larger structures. We have recently observed similar undulations for surfactant lamellar phases in brine near mica surfaces.[58] Here the undulation period depended on the membrane concentration (longer periods for lower concentrations) but was always larger than the distances noted here for the n-alkanols.

AM-AFM images of the near surface structure of PAN + octanol (column 2 of Figure 2) show a similar structural progression as a function of concentration. The structure of PAN + 10 vol% octanol is similar to that of the pure IL[33] and 1-butanol systems at low concentrations (≤50 vol %), but the polar domain centre to centre distance and size are both larger than for PAN + 10 vol% butanol. The first result is consistent with the greater increase in the apolar vol : polar vol when octanol is added instead of butanol (c.f. Table 1). However, the increase in the polar domain size is counter to this argument. Polar regions would be expected to be the same size as PAN + 10 vol% butanol (and pure PAN) due to the added polar volume being smaller for octanol than butanol. We attribute this apparent contradiction to changes in the preferred curvature of the nanostructure. While the C_4 chain of butanol can be incorporated readily into existing PAN monolayers with minimal disruption to the nanostructure, the C_8 chain of octanol cannot. An octyl chain is more than twice as long as that of the propyl cation, requiring a swelling of the (locally) bilayer apolar domain structure, or entropic confinement by coiling or "running along" the apolar domain. In either case this difference alters the curvature of PAN's nanostructure, which leads to larger polar domains seen in the AM-AFM image of PAN + 10 vol% octanol.

The average polar domain size decreases from 2.6 nm for PAN + 10 vol% octanol to 2.1 + 30 vol% octanol, c.f. Figure 3. For the butanol systems, the aggregate size decreases between 50 vol% and 70 vol% due to the nanostructure of PAN fragmenting. The same effect is unlikely for 30 vol% octanol due to the much lower

n-alkanol vol%. However, SAXS reveals that between 10 vol% and 20 vol% octanol begins to self-assemble into aggregates with length scales significantly larger than pure PAN.[33] This behaviour is reminiscent of the 'solvophobic de-mixing' postulated by Weingärtner *et al.* in ethylammonium nitrate / octanol systems.[59] The octanol aggregates are hydrocarbon rich meaning they will be compliant to the AM-AFM tip. This means they appear as dark regions in Figure 2, but because the eye is naturally drawn to light features are difficult to discern. To compensate, in Figure A of the Supplementary Information (SI) Figure 2 is reproduced but with the colour scales reversed, such that compliant regions are bright and noncompliant regions dark. In this image, the light octanol structures are clear, intermixed with smaller dark regions indicating the location of the polar domains of PAN. It must be emphasised that these structure are dynamic; there will be substantial intermixing of the different structures in time and space.

Increasing the 1-octanol concentration to 50 vol% produces larger polar domains (2.4 nm in diameter) with hints of smaller structures noted between the domains. The centre to centre spacing increases to 6.8 nm (Figure 3) and the polar domains appear more isolated than at 30 vol%. Comparison of the reverse contrast images presented in Figure A of the SI for PAN + 30 vol% octanol and PAN + 50 vol% octanol reveals that the (bright) octanol aggregates have markedly increased in size, and the dark domains indicating the PAN polar phase are more isolated. This is in good agreement with the X-ray scattering data obtained at similar concentrations[12] where the peak due to octanol structures moves to lower Q, becomes more intense and sharpens slightly.

When the octanol concentration is raised to 70 vol% the contrast between the compliant and noncompliant domains is reduced in Figure 2. This makes features more difficult to distinguish and Figure 3 reveals that around this concentration the aggregate size decreases as the solution structure tends towards that of pure octanol. The image in figure 2 is consistent with isolated PAN rich domains within a weakly undulating octanol rich matrix.

The features of the dodecanol images are strikingly different to that of pure PAN at all vol%. This is consistent with the SAXS data, which reveals structures much larger than that of PAN for all dodecanol concentrations studied (between 10 vol% and 90 vol%).

The size of the polar domains for 10 vol% dodecanol in Figure 2 are substantially larger than those in the corresponding octanol and butanol systems, c.f. Figure 3. This is attributed to dodecanol lowering the preferred curvature in the same fashion as described for 10 vol% octanol, but the effected is enhanced by dodceanol's longer alkyl chain. Examination of reverse contrast image for 10 vol% dodecanol (Figure A in the SI) reveals some large, discrete, light structures which indicate dodecanol rich aggregates. Dodecanol self assembles at lower concentrations than octanol because the longer alkyl chain responds more strongly to solvophobic effects. As the dodecanol concentration is increased to 30 vol% and 50 vol%, the features associated with the dodecanol aggregates become larger and more interconnected, while the polar domain size increases slightly but becomes more discrete. Both effects are due to the larger, more elongated dodecanol rich structures flattening the polar domains of PAN as it attempts to match the aggregate curvature. These results are consistent with the SAXS spectra.

The image for PAN + 70 vol% dodecanol reveals large domains superimposed upon smaller structures ~1 nm in diameter. The large domains (between 4 nm – 20 nm) have appearance similar to pure dodecanol in the image below, and are attributed to dodecanol rich regions in the mixture adopting a similar structure. The smaller structures are spaced ~ 1 nm apart in a hexagonal lattice and were present for this composition across multiple repeats with different tips. While the lattice structure is consistent with the underlying mica, the dimension is twice as large which negates the possibility that the adsorbed layer is imaged through the near surface structure. The origin of these small features is difficult to discern, but is indicative of small, isolated PAN rich clusters within the octanol rich matrix. However, SAXS spectra collected at similar concentrations showed no evidence of these small structures, suggesting that there are somehow templated by the adsorbed layer. Shear force data collected for 70 vol% dodecanol is the same within error as that for corresponding octanol and butanol systems.[50] This makes it unlikely that these small structures interact especially strongly with the adsorbed layer.

Conclusions

AM-AFM has been used to reveal how the near surface nanostructure of PAN + n-alkanol mixtures varies with n-alkanol vol% and chain length for butanol, octanol and dodecanol. The sensitivity of AM-AFM can

distinguish between near surface regions rich in polar groups, apolar groups, and n-alkanol aggregates when they are present.

The similar alkyl chain lengths of butanol and the propylammonium cation means that for concentrations up to 50 vol% butanol can pack into the native PAN nanostructure, causing swelling with minimal structural variation. When the butanol concentration is increased to 70 vol% the sponge structure fragments and smaller PAN rich aggregates are dispersed in a butanol rich matrix.

The longer alkyl chain length of octanol produces different structures. The octanol alkyl chain is too long to simply pack into the nanostructure of PAN like butanol. Even if the octanol's alcohol group is solvated in the polar domain the octanol alkyl chain is sufficiently long that it can transverse the apolar domain or run along it. This causes the PAN nanostructure to flatten and more elongated structures are noted in the images. Self-assembled octanol aggregates are present in the 30 vol%, 50 vol% and 70 vol% images. The aggregates size increases notably between 30 vol% and 50 vol%.

Dodecanol's longer alkyl chain means the effects noted for octanol are more pronounced and occur at lower concentrations. Dodecanol flattens the PAN nanostructure more strongly than octanol, especially at lower concentrations. The longer alkyl chain also means that dodecanol responds more strongly to solvophobic effects than octanol, and aggregates are noted even at 10 vol%. Near the surface of these aggregates, the nanostructure of the PAN rich matrix flattens as it attempts to match the aggregate curvature. This flattening effect decays with distance from the aggregate, but leads to larger average polar domain sizes.

Images for the pure n-alkanols are also presented. Membrane undulations can be discerned for dodecanol and octanol, and perhaps for butanol. These undulations become clearer and larger as the n-alkanol hydrocarbon chain length is increased, consistent with larger structures and stronger lateral interactions between n-alkanols in near surface bilayers.

Supplementary Information

Additional AM-AFM images are provided in the electronic supporting information. This material is available free of charge *via* the Internet at http://rsc.org

Acknowledgements

R.A. thanks the Australian Research Council Future Fellowship (FT120100313). This research was supported by an Australian Research Council Discovery Project (DP120102708) and Equipment Grant (LE110100235).

References

1. T. Welton, *Chem. Rev.*, 1999, 99, 2071-2083.
2. R. Hayes, G. G. Warr and R. Atkin, *Chem. Rev.*, 2015, DOI: 10.1021/cr500411q.
3. T. L. Greaves and C. J. Drummond, *Chem. Rev.*, 2008, 108, 206-237.
4. J. S. Wilkes, *Green Chem.*, 2002, 4, 73-80.
5. J. N. A. Canongia Lopes and A. A. H. Padua, *J. Phys. Chem. B*, 2006, 110, 3330-3335.
6. R. Hayes, S. Imberti, G. G. Warr and R. Atkin, *J. Phys. Chem. C.*, 2014, 118, 13998-14008.
7. R. Hayes, S. Imberti, G. G. Warr and R. Atkin, *Phys. Chem. Chem. Phys*, 2011, 13, 3237-3247.
8. R. Hayes, S. Imberti, G. G. Warr and R. Atkin, *Phys. Chem. Chem. Phys*, 2011, 13, 13544-13551.
9. C. Hardacre, J. D. Holbrey, C. L. Mullan, T. G. A. Youngs and D. T. Bowron, *J. Chem. Phys.*, 2010, 133, 74510 - 74517.
10. G. W. Stewart and R. M. Morrow, *Physical Review*, 1927, 30, 232-244.
11. O. Russina, A. Sferrazza, R. Caminiti and A. Triolo, *The Journal of Physical Chemistry Letters*, 2014, 5, 1738-1742.
12. H. J. Jiang, P. A. FitzGerald, A. Dolan, R. Atkin and G. G. Warr, *J. Phys. Chem. B*, 2014, 118, 9983-9990.
13. R. Hayes, G. G. Warr and R. Atkin, *Phys. Chem. Chem. Phys*, 2010, 12, 1709-1723.
14. R. S. Payal and S. Balasubramanian, *ChemPhysChem*, 2012, 13, 3085-3086.
15. R. S. Payal and S. Balasubramanian, *ChemPhysChem* 2012, 13, 1764-1771.
16. D. Dragoni, N. Manini and P. Ballone, *ChemPhysChem*, 2012, 13, 1772-1780.
17. N. Sieffert and G. Wipff, *J. Phys. Chem. C.*, 2008, 112, 19590-19603.
18. P. Rajdeep Singh and B. Sundaram, *J. Phys.: Condens. Matter.*, 2014, 26, 284101.
19. K. Shimizu, A. Pensado, P. Malfreyt, A. A. H. Padua and J. N. Canongia Lopes, *Faraday Discussions*, 2012, 154, 155-169.
20. S. Li, K. S. Han, G. Feng, E. W. Hagaman, L. Vlcek and P. T. Cummings, *Langmuir*, 2013, 29, 9744-9749.
21. J. L. Bañuelos, G. Feng, P. F. Fulvio, S. Li, G. Rother, N. Arend, A. Faraone, S. Dai, P. T. Cummings and D. J. Wesolowski, *Carbon*, 2014, 78, 415-427.
22. N. Manini, M. Cesaratto, M. G. Del Pópolo and P. Ballone, *J. Phys. Chem. B*, 2009, 113, 15602-15609.
23. L. Liu, S. Li, Z. Cao, Y. Peng, G. Li, T. Yan and X.-P. Gao, *J. Phys. Chem. C.*, 2007, 111, 12161-12164.
24. K. C. Jha, H. Liu, M. R. Bockstaller and H. Heinz, *J. Phys. Chem. C.*, 2013, 117, 25969-25981.
25. T. P. C. Klaver, M. Luppi, M. H. F. Sluiter, M. C. Kroon and B. J. Thijsse, *J. Phys. Chem. C.*, 2011, 115, 14718-14730.
26. A. C. F. Mendonça, A. A. H. Pádua and P. Malfreyt, *Journal of Chemical Theory and Computation*, 2013, 9, 1600-1610.

27. H. Valencia, M. Kohyama, S. Tanaka and H. Matsumoto, *Phys. Rev. B.*, 2008, 78, 205402.
28. F. Buchner, K. Forster-Tonigold, B. Uhl, D. Alwast, N. Wagner, H. Farkhondeh, A. Groß and R. J. Behm, *ACS Nano*, 2013, 7, 7773-7784.
29. B. Uhl, T. Cremer, M. Roos, F. Maier, H.-P. Steinruck and R. J. Behm, *Phys. Chem. Chem. Phys*, 2013, 15, 17295-17302.
30. T. Waldmann, H.-H. Huang, H. E. Hoster, O. Höfft, F. Endres and R. J. Behm, *ChemPhysChem*, 2011, 12, 2565-2567.
31. G.-B. Pan and W. Freyland, *Chem. Phys. Lett.*, 2006, 427, 96-100.
32. F. Endres and S. Z. El Abedin, *Zeitschrift Fur Physikalische Chemie-International Journal of Research in Physical Chemistry & Chemical Physics*, 2007, 221, 1407-1427.
33. A. Elbourne, K. Voitchovsky, G. G. Warr and R. Atkin, *Chemical Science*, 2015, 6, 527-536.
34. A. Elbourne, S. McDonald, K. Voïchovsky, F. Endres, G. G. Warr and R. Atkin, *ACS Nano*, 2015, DOI: 10.1021/acsnano.5b02921.
35. A. J. Page, A. Elbourne, R. Stefanovic, M. A. Addicoat, G. G. Warr, K. Voitchovsky and R. Atkin, *Nanoscale*, 2014, 6, 8100-8106.
36. J. J. Segura, A. Elbourne, E. J. Wanless, G. G. Warr, K. Voitchovsky and R. Atkin, *Phys. Chem. Chem. Phys*, 2013, 15, 3320-3328.
37. A. Elbourne, J. Sweeney, G. B. Webber, E. J. Wanless, G. G. Warr, M. W. Rutland and R. Atkin, *Chem. Commun.*, 2013, 49, 6797-6799.
38. R. Atkin and G. G. Warr, *Journal of Physical Chemistry C*, 2007, 111, 5162-5168.
39. S. Perkin, L. Crowhurst, H. Niedermeyer, T. Welton, A. M. Smith and N. N. Gosvami, *Chem. Commun.*, 2011, 47, 6572-6574.
40. H. Judith, H. Florian, H. M. Martin and B. Roland, *J. Phys.: Condens. Matter.*, 2014, 26, 284110.
41. M. Mezger, S. Schramm, H. Schröder, H. Reichert, M. Deutsch, E. J. De Souza, J. S. Okasinski, B. M. Ocko, V. Honkimäki and H. Dosch, *J. Chem. Phys.*, 2009, 131, -.
42. M. Tomitori and T. Arai, *Applied Surface Science*, 1999, 140, 432-438.
43. J. E. Sader, I. Larson, P. Mulvaney and L. R. White, *Rev. Sci. Instrum.*, 1995, 66, 3789-3798.
44. R. García, in *Amplitude Modulation Atomic Force Microscopy*, Wiley-VCH Verlag GmbH & Co. KGaA, 2010, DOI: 10.1002/9783527632183.ch6, pp. 77-90.
45. P. Duhamel and M. Vetterli, *Signal Processing*, 1990, 19, 259-299.
46. B. James and H. James, in *Dekker Encyclopedia of Nanoscience and Nanotechnology, Second Edition - Six Volume Set (Print Version)*, CRC Press, 2008, DOI: doi:10.1201/NOE0849396397.ch192, pp. 2211-2228.
47. S.-H. Loh and S. P. Jarvis, *Langmuir*, 2010, 26, 9176-9178.
48. J. A. Smith, G. B. Webber, G. G. Warr and R. Atkin, *J. Phys. Chem. B*, 2013, 117, 13930-13935.
49. N. V. Sastry and M. K. Valand, *J. Chem. Eng. Data.*, 1996, 41, 1426-1428.
50. J. Sweeney, G. B. Webber and R. Atkin, *Phys. Chem. Chem. Phys*, 2015, Submitted.
51. T. Murphy, L. M. Varela, G. B. Webber, G. G. Warr and R. Atkin, *J. Phys. Chem. B*, 2014, 118, 12017-12024.
52. J. Israelachvili, *Intermolecular and Surface Forces, Third Edition*, Academic Press, 2010.
53. H. V. R. Annapureddy, H. K. Kashyap, P. M. De Biase and C. J. Margulis, *J. Phys. Chem. B*, 2010, 114, 16838-16846.
54. K. S. Vahvaselka, R. Serimaa and M. Torkkeli, *Journal of Applied Crystallography*, 1995, 28, 189-195.
55. M. Tomšič, A. Jamnik, G. Fritz-Popovski, O. Glatter and L. Vlček, *J. Phys. Chem. B*, 2007, 111, 1738-1751.
56. H. J. Butt, B. Cappella and M. Kappl, *Surf. Sci. Rep.*, 2005, 59, 1-152.
57. V. Franz and H.-J. Butt, *J. Phys. Chem. B*, 2002, 106, 1703-1708.
58. M. J. Wydro, G. G. Warr and R. Atkin, *Langmuir*, 2015, DOI: 10.1021/acs.langmuir.5b01008.
59. H. Weingärtner, T. Merkel, S. Käshammer, W. Schröer and S. Wiegand, *Berichte der Bunsengesellschaft für physikalische Chemie*, 1993, 97, 970-975.

Graphical Abstract

50 Vol% PAN + 50 Vol% n-Alkanol Mixtures

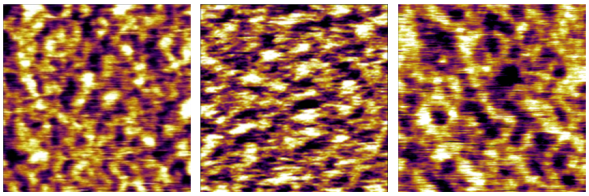

Butanol **Octanol** **Dodecanol**